**Supplementary Information**

**Supplementary legend for Figure 2**

(a) A 170 minute long recording was split in two files. Each file was normalized by its standard deviation and their spectra were averaged together and smoothed out with a median filter of rank 6.

(b) (Black line) Binary time series were divided into 5 min-length-intervals resulting in 222 binary time series. The resulting 222 power spectra were averaged together. (grey line) Binary time series were recorded from 16 different cells and divided into 5 min-length-intervals. The power spectra of the 45 resulting binary time series (normalized by their standard deviations) were averaged together.

(inset) The spectrum was computed from the average of 222 5-minute long binary time series.

(c) CW and CCW histograms (bin size= 0.1) were respectively normalized by the total number of CW and CCW intervals. CW (grey) distribution exhibits an exponential behaviour whereas CCW (black) lengths distribution displays a fat tail.

**Supplementary legend for Figure 3**

(a) CheR was expressed from the lac inducible plasmid pUA4 with varying levels of IPTG induction in RP4968 deleted strain for cheR[1]. (black) Average of 29 spectra. Dark grey: Average of 31 spectra. Grey: average of 34 spectra. Light grey: average of 40 spectra. For all the curves, after averaging the power spectra where smoothed out with a median filter of rank 2. (inset) grey: average of 44 power spectra No smoothing.

(b) Histograms were normalized by the total number of intervals for each [CheR] from the same RP4968 mutant cells as in panel (a). The CW length intervals exhibited an exponential distribution that did not change upon variations of [CheR] (data not shown).

(c) Fluctuations of the CW bias as a function of time. 700 seconds of data are plotted. The bias was defined as the fraction of time the bead span CW within a 30 seconds moving window. The maximum of the fluctuations about the mean across the population of 40 wild-type cells ranged about 86% ± 28.

**Supplementary Methods**

**RP4968 strain.** The relation [CheR] to IPTG was [CheR]/X = {13*[IPTG]/(15μM+[IPTG])}+1, where X was the basal level of expression with pUA4[2]. When [IPTG]=0μM and [CheR]/X~1, wild-type behaviour was recovered [CheR]/X~1. When [IPTG]=5μM and [CheR]/X ~ 4, the correlated noise was mostly eliminated. Finally, when [IPTG]=30μM and [CheR]/X ~ 10, cells exhibited only white noise. In agreement with the simulations, an increase of 4 folds wild-type [CheR] level was enough to flatten the slope in the power spectrum at time scales longer than 10 seconds.

**Assay**. Bacteria were immobilized onto microscope slides so that some of the flagella were free to rotate. Flagella were marked with micro-beads to visualize their rotation with a dark-field illumination[3]. The trajectory of a bead attached to a single flagellum was monitored using a photosensitive quadrant detector (Figure 1). A red filter was placed in the light path to protect bacteria from harmful blue radiation. An iris was positioned at the back focal plane of a 100x objective lens (UplanFl, 100×/1.30, Olympus, Japan) in order to reduce the field of view of the rotating bead. A 50-50% beam splitter split the light between a CCD camera (1/3" mid-resolution Exview digital B/W camera, Sony) and a 4-quadrant photomultiplier (Hamamatsu Photonics K.K., Electron Tube Center, type: R5900U-01-M4). Plano-convex lenses (focal length = 50mm) were used to magnify 5 fold the image of the bead in order to make the detection more sensitive to small displacements. The signal from the PMT was acquired with a computer board (PCI-6024E; 200 kS/s, 12-Bit. National Instrument, Austin, Texas). The length of the time series used to compute all the power spectra (except figure 2a) was 5 min.

**Spectral analysis of the chemotaxis network**

Noise analysis of chemical systems can be used to infer time scales involved in underlying molecular reactions[4]. Consider for example a simple isomerization between two species A and B (below) for which the relaxation time $\tau$ of the isomerization process is $\tau=1/(k+k')$. The time variations of the concentration of the species A with two different $\tau$ is plotted below (A(t)), left panel). Although the two time series exhibit fluctuations about the mean with similar amplitudes, the one with a shorter $\tau$ (grey line) fluctuates more rapidly. As a consequence, the fast process (grey) reaches its steady state faster than the slow process (black line). Difference in noise between the two processes can be visualized by filtering out high frequencies from the signal (middle panel). Filtering was carried out by averaging the time series with a moving window of chosen width (the time scale for this width is indicated by the full vertical line in the right panel). A more quantitative way to study the noise of a chemical process is to carry out spectral analysis of the temporal variations of concentrations. The flat portion of the power spectrum corresponds to the time scales for which the process is steady. The bend where the profile turns into a negative slope defines the relaxation time ($\sim 2\pi\tau$) of the system (arrows). At time scales smaller than $2\pi\tau$ the power spectrum is not flat and the process is unsteady. If the kinetic rates are decreased by a factor of 100, the bend is proportionally leftward-shifted (right panel).

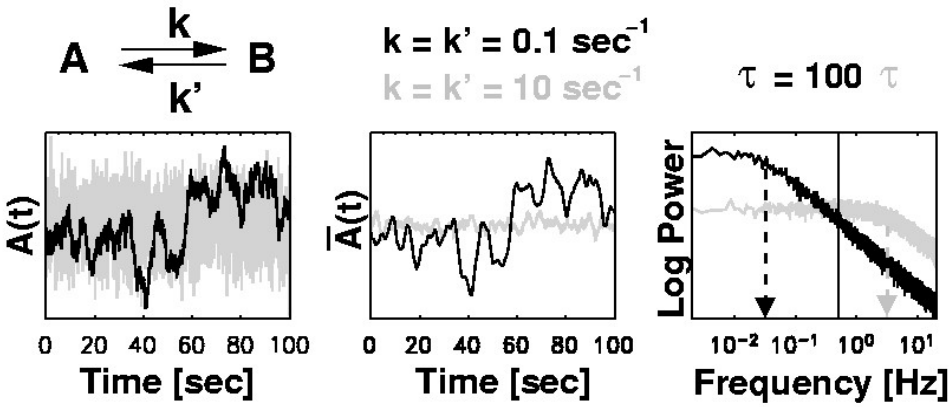


The chemotaxis system involves more than one single time scale. In our model (figure below), a feedback loop controls the phosphorylation of the response regulator CheY. This feedback mechanism depends on a pair of cytosolic enzymes, CheR (R) and CheB[5] (B), which respectively add and remove (with a time scale $\tau_m$) methyl groups at multiple receptor residues[6]. The activity of a receptor-associated kinase complex E* (E when inactive), which donates (time scale $\tau_p$) phosphate to CheY, increases with the number of methyl groups at these sites ($E_i$*, with i=0,1,2,3,4). Negative feedback is achieved through a parallel phosphotransfer (time scale, $\tau_p$) from $E_i$* to CheB (Bp) that in turn enhances the demethylation activity[7]. The activity of the receptor-kinase complex (E*), can vary very rapidly due to conformational changes of the receptors (time scale $\tau_c$). Phosphorylated CheY (Yp) binds preferentially to the cytoplasmic base of the motors that switch between two rotational modes (clockwise, CW, and counter-clockwise, CCW). CheZ, a phosphatase, removes phosphate from CheY-p (timescale $\tau_p$). When the concentration of CheY-P increases, motors spend more time spinning clockwise. The (de)methylations are the slowest reactions in the network ($\tau_m >> \tau_p, \tau_c$). Spectral analysis of the network output (CheYp) allows the identification of several characteristic timescales of this signalling pathway.

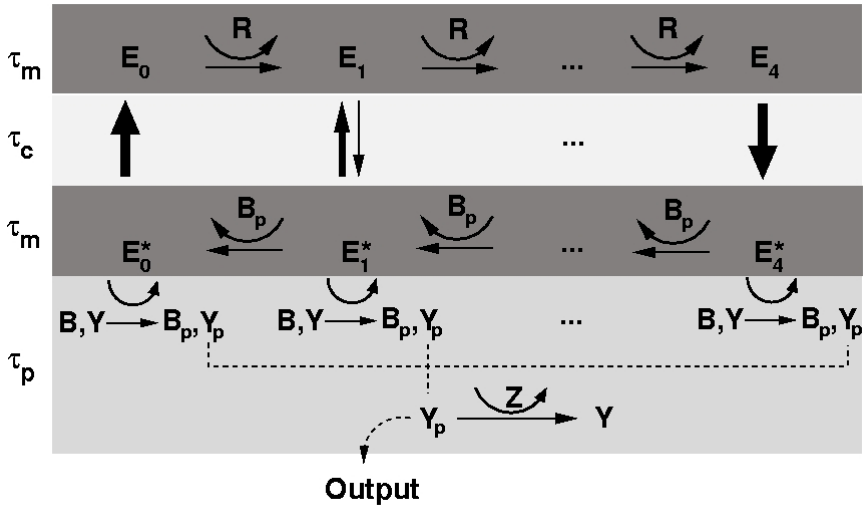

Some details on the numerical simulations: Important features of the numerical model are as follows. The Tar-CheW-CheA complex can be in an active or inactive conformation. Auto-phosphorylation of CheA occurs only when the receptor complex is in its active conformation. The probability to be in either conformation depends on the methylation level of the Tar receptor. The motor was not included in this model: the output of the chemotaxis network in our stochastic simulations was the number of CheYp proteins as a function of time. This was different from the experimental data for which the network output was defined as the switching events from an individual bacterial motor. Power spectra of the output of the mutant PS2001 (Fig. 2B), however, indicated that the motor alone did not generate correlated fluctuations at frequencies lower than 1 Hz. Comparison of power spectra from our model with the experimental data is therefore significant.

**Origin of the correlated noise.** To investigate the origin of the correlated noise in the numerical model (slope, flats), we computed the power spectrum of the signal at different levels within the pathway. The approximate Lorenzian shape of the power spectrum around $\nu \sim 10^{-3}$ Hz results from the fluctuations in the mean methylation level of the receptors. The relaxation time $\tau_m$ of the methylation /demethylation of the receptors corresponds to the change of slope ($\tau_m \sim 1000$ secs for wild-type (see also Box 1). It is possible that stochastic processes present in a living bacterium, but not incorporated in the numerical model, are also contributing to the experimental fluctuations depicted in Figures 2 and 3. Examples include the effects of diffusion on the rate of CheR-catalyzed methylation reactions, and the recently proposed inter-receptor interactions within the observed clusters of chemotactic receptors. However, regardless of the source of these correlated fluctuations, these simulations demonstrate that the downstream chemotaxis network allows the propagation of the "colored noise" to produce non-stationary behaviour. Experimental and theoretical studies have demonstrated that for reversible bimolecular reactions of the form $A+B \leftrightarrow C$ with $[A] << [B]$ (and A and C molecules immobile and B molecules mobile), the relaxation kinetics to equilibrium follow a power law, rather than simple exponential decay.

**Foraging behaviour.** There is a striking similarity between our results, in which power laws arise around an optimal value of [CheR], with that of a recently proposed theory for explaining the ubiquity of power laws in nature and engineered systems. This theory suggests that power-law distributions emerge from engineered or evolved designs of systems with optimal behaviour[8,9]. It is also common to think that an optimized random search of a forager involves a distribution of flight lengths characterized by one length scale with a well-defined variance. For example, this would be the case in bacterial chemotaxis if run lengths (flight lengths) were to be exponentially distributed. In contrast, it was recently reported[10] that the best statistical strategy to search efficiently in two dimension for randomly located targets is achieved with “an inverse square power-law distribution of flight lengths”[10] (Fig. 2c). To illustrate the potential advantage of power-law distributions of CCW intervals for foraging behaviour, we simulated 3D trajectories using as input the binary time series of switching event measured from wild-type and mutant cells. One limitation in relating the data from individual motors into tumbling events of swimming cells is that not every switching event translates into a run/tumble transition[11]. The statistics of switching,

therefore, may not be directly comparable with the run/tumble data. It may be possible that the run/tumble statistics are much closer to exponential even if the distribution of CCW events from individual motors exhibits heavy tails or power-law behaviour. Nevertheless, we artificially constructed 3-dimensional trajectories from the measured binary time series of switching events of individual motors.

We found two distinct swimming behaviours. The red trajectory (figure below) corresponds to 398 seconds of switching events measured from an individual motor in a wild-type cell (we used a subset from the data of the Figure 2a with CW bias =0.19, switching frequency =0.58 $sec^{-1}$). The blue trajectory (figure below) illustrates the motion of a mutant cell lacking the chemotaxis network. The binary time series used to produce the "blue" trajectory is a subset of the data set used to plot the grey curve in Figure 2b (CW bias = 0.20, switching frequency =0.71). As suggested by recent theories on optimal foraging behaviour, the power-law distribution produces trajectories that effectively cover several length scales whereas exponential distribution leads to trajectories for which the mean length of runs is the only explored length scale.

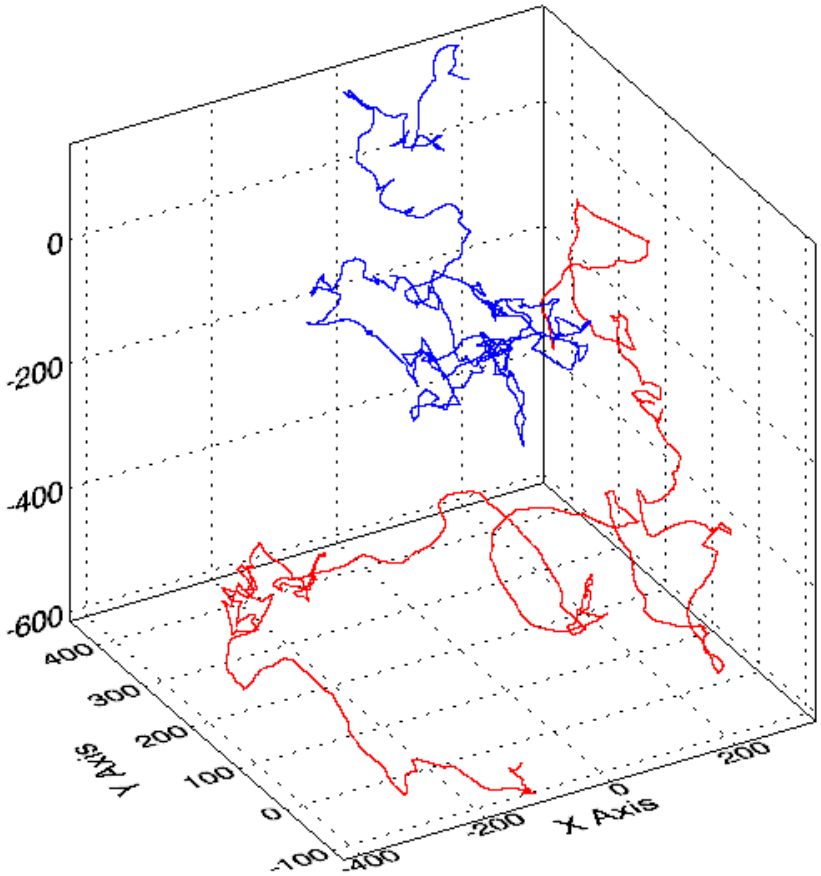


In this figure, lengths are given in micrometers. The binary time series of CW and CCW intervals were respectively converted into tumbles and runs. During a run (CCW rotation) the speed was held constant

(20 μm/sec) and the direction of motion was allowed to drift with rotational diffusion coefficient = 0.062 radian$^2$/sec (calculated for a sphere of radius 1μm at 305 ºK in a medium with viscosity 0.027 g cm$^{-1}$ sec$^{-1}$).[12] During a tumble (CW rotation), the position of the cell was held constant and a new direction of the motion was chosen randomly from one of the straight lines defining a cone with axis of symmetry along the original direction of motion and aperture angle α. The angle α was drawn from the distribution $p(\alpha)=\cos(\alpha/2)/2$, $0<\alpha<\pi$, ensuring a mean tumble angle of 65º degrees with the standard deviation of 43º (Berg & Brown[13] measured that the mean tumble angle for wild-type E Coli was 68º with a standard deviation of 36º).


1. Alon, U., Surette, M. G., Barkai, N. & Leibler, S. Robustness in bacterial chemotaxis. *Nature* **397**, 168-71 (1999).
2. U. Alon private communication from ref. 6.
3. Cluzel, P., Surette, M. & Leibler, S. An ultrasensitive bacterial motor revealed by monitoring signaling proteins in single cells. *Science* **287**, 1652-5 (2000).
4. McQuarrie, D.A., Keizer, J.E., "Fluctuations in Chemically Reacting Systems", Theoretical Chemistry: Advances and Perspectives, Volume 6A, pages 165-213 (1981).
5. Lupas, A. & Stock, J. Phosphorylation of an N-terminal regulatory domain activates the CheB methylesterase in bacterial chemotaxis. *J Biol Chem* **264**, 17337-42 (1989).
6. Stock, J., Surette, M. & Park, P. Chemosensing and signal transduction in bacteria. *Curr Opin Neurobiol* **4**, 474-80 (1994).
7. Bourret, R. B. & Stock, A. M. Molecular information processing: lessons from bacterial chemotaxis. *J Biol Chem* **277**, 9625-8 (2002).
8. Carlson, J. M. & Doyle, J. Highly optimized tolerance: Robustness and design in complex systems. *Physical Review Letters* **84**, 2529-2532 (2000).
9. Carlson, J. M. & Doyle, J. Complexity and robustness. *Proceedings of the National Academy of Sciences of the United States of America* **99**, 2538-2545 (2002).
10. Viswanathan, G. M. et al. Optimizing the success of random searches. *Nature* **401**, 911-914 (1999).
11. Turner, L., Ryu, W. S. & Berg, H. C. Real-time imaging of fluorescent flagellar filaments. *J Bacteriol* **182**, 2793-801 (2000).
12. Berg, H.C. Random walks in biology (Princeton University Press, Princeton, 1983)
13. Berg, H. C. & Brown, D. A. Chemotaxis in Escherichia coli analysed by three-dimensional tracking. *Nature* **239**, 500-4 (1972).